

Abass O. ALADE^{a,b,c}, Akeem Olatunde ARINKOOLA^a,
Tinuade J. AFOLABI^{a,c}, Adedayo Ayodele ADEGBOLA^d,
Olukayode Gideon OLOYEDE^{a,c}, Praise Osamuode ODIASE^{a,c}

D-OPTIMAL OPTIMIZATION OF MICROWAVE-ASSISTED SYNTHESIS OF MORINGA OLEIFERA POD ACTIVATED CARBON AND APPLICATION TO METHYLENE BLUE ADSORPTION

^a Department of Chemical Engineering, Ladoko Akintola University of Technology, Ogbomoso, NIGERIA

^b Science and Engineering Research Group (SAERG), Ladoko Akintola University of Technology, Ogbomoso, NIGERIA

^c Bioenvironmental Water and Engineering Research Group (BWERG), Ladoko Akintola University of Technology, Ogbomoso, NIGERIA

^d Civil Engineering Department, Ladoko Akintola University of Technology (LAUTECH), Ogbomoso, NIGERIA

Abstract: Activated carbon was optimally produced from Moringa oleifera pod (AMOP), with the aid of microwave, based on the D-Optimal Design under the Response Surface Methodology of the Design Expert software (6.0.8). Process factors selected were time (20–60 mins), temperature (200–450 °C), and impregnation ratio (IMR) (1:1-1:5), while the responses selected were yield, Methylene Blue Number (MBN) and Iodine Value Number (IVN). Adsorption, kinetic and diffusion mechanism of Methylene Blue (MB) adsorption on the AMOP were investigated. Suitability of types 1-6 of pseudo-second-order (PSO) equation was analysed. Surface properties of the AMOP were characterized using Fourier Transform Infrared Spectroscopy (FTIR) and physicochemical analysis. The optimum conditions (20 mins, IMR of 1:1, and 450 °C) obtained for the activation/carbonization gave 22.11% yield, 78.53 mg/g MBN and 96 mg/g IVN. The FTIR spectra showed changes in the functional groups on the AMOP after the activation/carbonization process. Maximum adsorption capacity of AMOP for MB adsorption was 98.46 mg/g. The process fit well to Type3 of PSO ($R^2 > 0.9$). The process's adsorption rate was controlled by diffusion mechanism. This study showed that Moringa oleifera pod is a viable precursor for the production of effective activated carbon.

Keywords: D-Optimal, Methylene Blue, Moringa oleifera pod, Optimization

1. INTRODUCTION

Activated carbons are carbonaceous materials that are characterized by extraordinary large specific surface areas and porosity as well as surface-containing functional groups (Baker et al., 1992). A wide variety of agricultural by-products and wastes such as coconut buttons (Anirudhan and Sreekumari, 2011), okra waste (Hashem, 2007), maize cobs and rice husks (Abdel-Ghani et al., 2007), and apple pulp (Garcia et al., 2003) have been investigated as cellulosic precursors for the production of activated carbon. These activated carbons are widely used for the removal of organic and inorganic pollutants of environmental concern from contaminated air, gases, and water (El-Hendawy, 2003). The effectiveness of these activated carbons has led to increased research on agricultural wastes and leftovers as candidate precursors for the production of effective activated carbon (Ioannidou, and Zabaniotou, 2007)

Moringa oleifera is a perennial plant that grows very fast within twelve months of planting, up to a height greater than 5 m and produces pods which are more 30 cm long (Lilliehöök, 2005). All parts of Moringa oleifera tree are used for many different purposes and various studies have been carried out using different parts of the tree (Muyibi et al., 2002; Kabore et al., 2013; Sivakumar, 2013).

High quality oil have been obtained from *Moringa oleifera* dried seeds while the resulting pressed cake mixed have been used as coagulant for water treatment (McConnachie et al., 1996). The oil extracted from the seeds has been used for medicinal, cosmetics, soap, cooking purposes (Arora, et al., 2013). *Moringa oleifera* seed and its defatted cake show good coagulating properties, particularly, for control of pH, alkalinity and conductivity of the water compared to chemical coagulants (Sarpong, and Richardson, 2010). *Moringa oleifera* seed coagulant has been used for removing chemical oxygen demand (COD) and total dissolved solids (TDS) from municipal solid waste leachate (Sivakumar, 2013). *Moringa oleifera* seed powder was used for chromium, lead and cadmium ion removal from aqueous solution (Sharma, et al., 2006; 2007).

Methylene blue (MB) is one of the frequently used cationic dyes in dyeing industries and as result became one of the predominant pollutants in water stream (Amuda et al., 2014). MB treatment in aqueous solution has attracted much interest because of its structural stability and complexity, which has led to numerous detrimental effects on human health and environment (Njoku et al., 2014). Various methods such as biological treatment, coagulation, flotation, electrochemical techniques, adsorption, and oxidation have been adopted for MB removal from aqueous solution (Rashidzadeh et al., 2015). Adsorption techniques has proved effective due to its various advantages such as ease of operation and high removal efficiency (Han et al., 2015). Application of low-cost adsorbents such as silica, sewage sludge, industrial solid wastes, clay, agriculture waste and activated carbon, has advanced adsorption techniques for the removal of inorganic and organic pollutants including MB, at low cost (Rafatullah et al., 2010). In this study, activated carbon was optimally produced from *Moringa oleifera* pod (AMOP).

2. MATERIALS AND METHOD

— MATERIALS

The precursors, *Moringa oleifera* pods (MOPs), were sourced as waste from various moringa seed harvesting centers in Ogbomoso, Nigeria. Reagents used include distilled water, H_2SO_4 , Methylene blue, $Ca(OCl_2)$, $NaHSO_3$, ethanol, potassium iodide, starch indicator that were all of analytical grade.

— METHODS

Experimental Design

The selected ranges of temperature, time and impregnation ratio used for the activation/carbonization procedure were between 200 - 450 °C, 20 - 60 mins and impregnation ratio 1:1 - 1:5, respectively. These values fall within the ranges used in previous studies, and were run under the D-Optimal Design in the Design Expert (DOE) (6.0.8) software to generate experimental runs at random. The selected responses were yield, Methylene Blue Number (MBN) and Iodine Value Number (IVN) (Verla et al., 2012).

Activated Carbon preparation

The raw MOPs were washed with distilled water to remove sand and stones, oven-dried to constant weight, then ground to reduce its particle size and increase its surface area. The precursor was soaked in beaker containing acetic acid (0.1 M) for 12 h at different impregnation ratios (IMR) (1:1 - 1:5) (Eqn 1) (Ahmad et al., 2015). The impregnation process was enhanced with microwave oven at 150 Hz for 2 h, after which the mixture was heated on hot plate to form paste before oven-dried to a constant weight (Verla et al., 2012).

$$\text{Impregnation ratio (IMR)} = \frac{\text{Weight of activant}}{\text{Weight of precursor}} \quad (1)$$

Determination of Yield

The activated MOP (3 g) was measured into crucibles, which were charged into the muffle furnace at the designated time and temperature in the DOE software experimental design. The carbonized material was cooled to room temperature, washed thoroughly with distilled water to remove adhering ashes and then dried to constant weight at 105 °C for 72 hrs. The yield of the activated carbon obtained is expressed as ratio of the sample weight after pyrolysis, to the weight of the raw material (Lua et al., 2004) and the percentage yield of carbonized carbon was determined according to the method adopted by Salman, (2014) (Eqn 2). The experiment was conducted in triplicates and the average was used subsequently.

$$\text{Yield (\%)} = \frac{W_c}{W_o} \times 100 \quad (2)$$

where W_c and W_o are the dried weight of carbonized carbon and dried weight of precursor respectively.

Determination of Methylene Blue Number (MBN)

The adsorption capacity of the developed activated carbon *Moringa oleifera* pods (AMOP) was estimated using standard Methylene Blue Number (MBN) test. The amount of methylene blue adsorbed was determined by measuring 10 mg of the carbonized material in 10 ml of 100 mg/L of methylene blue solution for 24 h at room temperature (Hesas et al., 2013). The remaining concentration of unadsorbed methylene blue was analysed using UV/Vis spectrophotometer and the amounts adsorbed were evaluated using equation 3.

$$q_e = \frac{(C_0 - C_e) \times V}{m} \quad (3)$$

where C_0 (mg/L) and C_e (mg/L) are the methylene blue concentration at starting time ($t = 0$) and at equilibrium time respectively, V (L) is the volume of the solution treated and M (g) is the mass of adsorbent.

Determination of iodine value number (IVN)

The iodine value number (IVN) test was carried out by using standardized sodium thiosulphate producing a stock solution of iodine (2.7 g of iodine crystals and 4.1 g of potassium iodide in 1 L of distilled water) (Gimba, and Musa, 2007). The carbonized material (0.5 g) was weighed into 100 cm³ volumetric flask and 10 cm³ of 5% v/v HCl acid was introduced. The mixture was agitated to wet the carbonized material, effectively, before adding 100 cm³ of the freshly prepared iodine solution and agitated further at 200 rpm for 60 min. The mixture was filtered with Whatman filter paper and 20 ml of the filtrate was titrated with 0.1 M sodium thiosulphate, with starch as indicator. Equation 4 was employed to determine the concentration of iodine absorbed by the activated carbon at room temperature.

$$IVN = \frac{B-S}{B} \times \frac{VM}{W} \times 253.81 \quad (4)$$

where B is the volume of thiosulphate solution required for the blank, S is the volume of thiosulphate solutions required for the sample titrations, W is the mass of activated carbon sample, M is the concentration of the iodine solute, V is 20 ml aliquot and the atomic mass of iodine is given as 253.81.

Characterization

≡ Physico-chemical properties

The moisture content, bulk density and ash contents of the AMOP produced were analysed using a thermogravimetric Analyzer (TGA) (Perkin Elmer TGA7, US). The sample (5 g) was transferred into the platinum pan of the TGA, degassed for a few minutes and heated from ambient temperature to 110 °C until a constant weight was obtained for the moisture content determination. The temperature was later increased to 850 °C and kept constant for 7 min before being decreased to 800°C. The ash content and the remaining mass were determined at the end of the analysis (Bello et al., 2015).

≡ Fourier transforms infrared spectroscopy (FTIR)

Fourier transform infrared (FTIR-2000, Perkin Elmer) spectroscopic analysis was used to study the surface chemistry of the MOP and AMOP. General operation involved the discs preparation wherein 1 mg of dried sample was mixed with 0.5 g of KBr in an agate mortar and then pressed at 10 tonnes.cm⁻² for 15 min under vacuum. FTIR spectra were recorded between 4000 and 400 cm⁻¹ and the results obtained give information about the characteristic functional groups on the surface of raw and activated MOP (Bello et al., 2015).

— Batch Kinetic Experiments

The kinetics of methylene blue dye adsorption onto the AMOP was carried out by withdrawing each flask, containing 100 mg/L of MB and 0.1 g of AMOP, for analysis at 20 min interval until the determined concentrations are relatively closer. The amount adsorbed at time (t) was calculated according to eqn 5 (Ahmad et al., 2015).

$$q_t = \frac{(C_0 - C_t) \times V}{m} \quad (5)$$

where C_0 and C_t (mg/L) are the liquid phase concentrations of methylene blue at initial time ($t=0$) and time t ($t=t$), respectively, V (L) is the volume of the solution, and W (g) is the mass of dry adsorbent used.

Adsorption kinetics

Adsorption Kinetics is commonly modelled using the pseudo-kinetic models (El-Khaiary et al., 2010). The model generally simulates the overall rate of adsorption of a particular concentration

of adsorbate onto available surface of an adsorbent. The two most widely used kinetic models for describing the rate of adsorption of various organic and inorganic pollutants from wastewater streams are the Pseudo-first-order (PFO) and Pseudo-second-order (PSO) (Ahmad et al; 2015; Hirunpraditkoon et al., 2015).

≡ **Pseudo-first-order (PFO)**

The PFO model is given as

$$\frac{dq_e}{dt} = K_1(q_e - q_t) \tag{6}$$

where q_e ($mg\cdot g^{-1}$) and q_t ($mg\cdot g^{-1}$) are the amount of adsorbate onto adsorbent per unit mass of adsorbent at equilibrium and time t , respectively. K_1 (min^{-1}) represent the PSO rate constant (Ahmad et al, 2015; Hirunpraditkoon et al; 2015).

The PFO equation is integrated with initial condition of $q_t=0$ at $t=0$, And the resultant evaluation lead to two linear form given as equation 7 and 8

$$\log(q_e - q_t) = \log q_e - \frac{K_1}{2.303t} \tag{7}$$

$$\ln(q_e - q_t) = \ln q_e - K_1^{**}t \tag{8}$$

Plot of $\log(q_e - q_t)$ versus t as well as $\ln(q_e - q_t)$ versus t will give a straight line for the evaluation of K_1^* and K_1^{**} , respectively. The intercept $\log q_e$ and $\ln q_e$ give the calculated q_e , which is amount of adsorbate adsorbed at equilibrium q_e (mg/g) (Ahmad et al., 2015).

≡ **The pseudo-second-order (PSO) model**

The pseudo-second-order (PSO) model is given as

$$\frac{dq_e}{dt} = K_2(q_e - q_t)^2 \tag{9}$$

The terms, q_e , q_t and t are as described above while K_2 ($g\cdot mg^{-1}\cdot min^{-1}$) is the second-order rate constant. The integration of equation 8 has led to different linear forms (Type 1 - 6) Nouri et al., (2007) (Table 1). Nouri et al., (2007) reported the application of six linear types for removal of cadmium ions from aqueous base using wheat bran, while El-Khaiary (2010) reported the application of four linear types for the modelling of adsorption systems. Subah and Prasad (2015) applied four linear types to model sorption kinetics of titanium industry effluent on activated carbon. Type 1, which has been reported, extensively, in the work of Ho (Ho and McKay 2000; Ho et al., 2002; Ho and Ofomaja, 2006; El-Khaiary 2010) is most commonly used type of the PSO model equation. Blanchard et al., (1984) used the Type 6 successfully for ion exchange reaction on zeolite particles.

Table 1: Linear Forms of the Pseudo-Second-Order Kinetic Model

Type	Linear form	Plot
Type 1	$\frac{t}{q} = \frac{1}{k_2 q_e^2} + \frac{1}{q_e} t$	t/q vs. t
Type 2	$\frac{1}{q} = \frac{1}{q_e} + \frac{1}{k_2 q_e^2} \frac{1}{t}$	$1/q$ vs. $1/t$
Type 3	$q = \frac{1}{q_e} + \frac{1}{k_2 q_e^2} \frac{1}{t}$	q vs. q/t
Type 4	$\frac{q}{t} = k_2 q_e^2 - k_2 q_e q$	q/t vs. q
Type 5	$\frac{1}{t} = -k_2 q_e + k_2 q_e^2 \frac{1}{q}$	$1/t$ vs. $1/q$
Type 6	$\frac{1}{(q - q_c)} = \frac{1}{q_e} + k_2 t$	$1/(q_c - q)$ vs. t

This study used Type 1-5, to evaluate the adsorption of MB onto AMOP. Type 6 was not found to be suitable and this could be a good reason for its application in ion exchange reaction (Blanchard et al., 1984). The initial adsorption rate ‘ h ’ (expressed differently for Type 1-5) (Table 1), coefficient of determination (R^2) and the amount of MB adsorbed at equilibrium (q_e) were evaluated for the five types. Suitability of the type is usually base on the high R^2 values and the type with lower R^2 values, relatively, are considered unsuitable to describe adsorption rate of the system. R^2 represents the fit between the experimental data and linearized form of the model equations.

≡ **Elovich Kinetic Model**

The Elovich model equation is given as eqn 10 and simplified in linear form (eqn 11)

$$\frac{dq}{dt} = \alpha e^{-\beta q_t} \tag{10}$$

$$q_e = 1/\beta \ln(\alpha\beta) + (1/\beta) \ln t \tag{11}$$

when α is the initial adsorption rate (mg/min) and β is related to the extent of surface coverage and the activated energy for chemisorption (g/mg). Plot of q_t against $\ln t$ gives a straight-line relationship with a slope of $1/\beta$ and intercept of $1/\beta \ln(\alpha\beta)$. The number of site available for

adsorption is obtained as $1/\beta$ while the value of the intercept $\{1/\beta \ln(\alpha\beta)\}$ reflects the adsorption quantity (Ahmed et al., 2015).

Validity of Kinetic Model

The transformation of non-linear kinetic equations to linear forms affects their error structure. This alteration may eventually distort the error variance and standard least square method normality (Nouri et al., 2007). The error analysis of the PSO types was evaluated using equation 12, based on normalized standard deviation, rather than selecting suitable form based on low R^2 and reasonable closeness of calculated (q_{cal}), to experimental (q_{exp}). Lower value of Δq_e indicates good fit between experimental and calculated data (Inyinbor et al., 2016).

$$\Delta q_e(\%) = 100 \sqrt{\left[\frac{(q_{exp} - q_{cal})/q_{exp}}{N-1} \right]} \quad (12)$$

where n is the number of data points, q_{exp} and q_{cal} (mg/g) are the experimental and calculated absorption capacity value.

— Adsorption Diffusion Mechanism

Adsorption process is usually favoured with vigorous agitation to facilitated effective contact between the adsorbent and adsorbate. During the process, removal of adsorbate from liquid media onto the adsorbent usually takes place in three stages such as mass transfer of adsorbate from aqueous phase onto the surface of the adsorbent surface (film diffusion), internal diffusion of adsorbate through the pores of the adsorbent (pore or particle diffusion) and final adsorption of the adsorbate on the adsorbent surface sites (Podder and Majumder, 2016).

Weber-Morris Diffusion Model

The most widely used for studying intraparticle diffusion mechanism is the Weber-Morris diffusion model (Weber and Morris, 1963) given as

$$q_t = K_{WM}t^{0.5} + C \quad (13)$$

where K_{WM} is intra-particle diffusion rate constant, C is a constant, which reflects the boundary layer thickness and t , is the time (mg/g). Theoretically, if the plot of q_t versus t gives a straight line, the adsorption process is characterized by rate-limiting step, which indicate intraparticle diffusion (Doke and Khan, 2012). If the plot is characterized by linear plots, then the adsorption process involves more than one-step control (Doke and Khan 2012).

Dumwald-Wagner Model

The Dumwald-Wagner diffusion Model is given as

$$\log(1 - F^2) = \frac{-K_{DW}}{2.303} t \quad (14)$$

where F is the ratio of q_m to q_e (i.e. q_m / q_e), K_{DW} is the diffusion rate constant and t is time. Plot of $(1 - F^2)$ against t is to give a linear relationship, which is expected to pass through the origin, naturally, and K_{DW} is evaluated from the slope of the curve.

McKay Model

The McKay Model is called film diffusion mass transfer rate equation (McKay, et al., 1981), which is expressed as equation 15 (Podder and Majumder, 2017)

$$\ln(1 - F) = -K_M t \quad (15)$$

where F is given as q_m/q_e , K_M is the diffusion rate constant and t is time. K_M is evaluated as slope of the plot of $\ln(1 - F)$ against t .

Bangham's Model

The Bangham's model is also known as the Double Logarithm Model (Podder and Majumder, 2017) and it is given as

$$\log \left[\log \left(\frac{C_0}{C_0 - q_t} \right) \right] = \log \left(\frac{K_b}{2.303V} \right) + \alpha_b \log(t) \quad (16)$$

where C_0 is the initial concentration of methylene blue solution (mg/L), q_t is the quantity of methylene blue adsorbed at time t , M is the mass of adsorbent (g/L), V is the volume of methylene blue solution in mL, while α_b and K_b are constants obtainable from slope and intercept, respectively.

3. RESULTS AND DISCUSSION

— Model Summary for the Production of Moringa oleifera Pod Activated Carbon

The study category used for the experimental design in the production of AMOP was D-optimal Design, under Response Surface Methodology (RSM). The factors considered were temperature (A),

time (B) and impregnation ratio IMR (C), while the responses were yield (Y_1), Methylene blue number MBN (Y_2) and Iodine value number IVN (Y_3). Eighteen (18) experimental runs were generated and power ($\lambda=2$) as well as inverse transformation were done for the yield and MBN, respectively. Cubic model showed the least standard deviation of 320.09 as well highest R^2 (0.9965) and Adjusted R^2 (0.9850). However, no value was generated for its Predicted R^2 , thus the model was aliased. The model with the next lowest standard deviation, highest R^2 , Adjusted R^2 and Predicted R^2 was considered, quadratic model was selected for the Yield. Similar trend was advanced for the suggested quadratic and 2-Factor Interaction (2FI) models for MBN and IVN, respectively.

— Responses from Experimental Data

The responses at different temperature, time and impregnation ratio conditions as generated by the software (Design Expert 6.0.8) (Table 2). Highest carbon yield (88.9%), MBN value (86.58 mg/g) and IVN value (96 mg/g) were obtained at Run 6 (200 °C, 20 mins and 1:1 IMR), Runs 7/15 (200 °C, 60 min and 1:5 IMR) and Run 8 (450 °C, 20 mins and 1:1 IMR), respectively. The lowest yield (9.9%), MBN value (27.24 mg/g) and IVN value (64 mg/g) were obtained at Run 11 (450 °C, 60 min and 1:1 IMR), Runs 14/17 (450 °C, 60 min and 1:5 IMR), and Runs 14/17 (450 °C, 60 mins and 1:5 IMR), respectively. The conditions selected for the activation/carbonization process are 450 °C, 20 mins and 1:1 impregnation ratio (Run 8) (Table 2). The selection was based on the relatively high values obtained for the IVN and MBN tests (96 mg/g and 78.53 mg/g respectively) as well as a yield value of 22.1%, which lies between the acceptable yield ranges (15 - 30%) (Alade et al., 2012a).

Table 2: Results of Responses from Experimental Data

Runs	Factors			Responses		
	Temperature (°C)	Time (mins)	IMP	Yield (%)	MBN (mg/g)	IVN (mg/g)
1	450.00	20.00	5.00	20.22	66.42	90
2	450.00	20.00	5.00	20.22	66.42	90
3	325.00	40.00	5.00	31.66	78.13	92
4	200.00	40.00	1.00	63.85	84.87	66
5	450.00	60.00	1.00	31.66	37.39	70
6	200.00	20.00	1.00	88.88	69.43	78
7	200.00	60.00	5.00	71.84	86.58	76
8	450.00	20.00	1.00	22.11	78.53	96
9	200.00	60.00	1.00	63.33	85.20	80
10	200.00	20.00	5.00	87.66	65.77	76
11	450.00	60.00	1.00	9.88	37.39	70
12	450.00	40.00	3.00	21.55	47.31	76
13	325.00	60.00	3.00	33.67	76.82	76
14	450.00	60.00	5.00	11.00	27.23	64
15	200.00	60.00	5.00	71.67	86.58	76
16	262.50	30.00	3.00	45.44	85.20	72
17	450.00	60.00	5.00	11.00	27.23	64
18	325.00	20.00	1.00	39.89	81.78	68

IMR- impregnation ratio IVN- iodine value number MBN – methylene blue number

— Analysis of variance (ANOVA)

The model equation developed is significant with F-value of 25.64, which suggest a 0.01% chance of occurrence due to noise (Table 3). A, B, A² and AB are the significant model term at P < 0.05. Lack of Fit F-value of 8.49 indicating 3.10% chance of occurrence due to noise and it implies that the Lack of Fit is significant relative to the pure error. The standard deviation, mean, coefficient of variation (C.V.), R^2 , Adjusted (Adj) R^2 , and predicted (pred) R^2 obtained from the analysis were 697.07, 2382.21, 29.26, 0.9665, 0.9288, and 0.7804, respectively. The Pred R^2 (0.7804) is in reasonable agreement with the Adj R^2 (0.9288) and Adequate (Adeq) Precision of 15.399, which is greater than 4, was found desirable to navigate the design space (Salman 2014).

The ANOVA for MBN shows that suggested model with, F-value of 34.47, is significant (Table 3) and the significant model terms are A, B, C, A², AB, AC and AB. The standard deviation, mean, C.V, R^2 , Adj R^2 , pred R^2 and Adeq precision were 1.951×10^{-3} , 0.018, 11.08, 0.9749, 0.9466, 0.8091, and 17.927, respectively. The Pred R^2 (0.8091) is in reasonable agreement with the Adj R^2 (0.9466)

and Adeq Precision of 17.927 (> 4) indicated the tolerability of the model for the experimental design. The analysis for the IVN based on ANOVA for response surface 2FI Model (Table 3) suggests that the Model F-value of 3.36 which is significant indicate a 3.92% chance of occurrence due to noise.

Table 3: Analysis of Variance (ANOVA) for the Percentage Yield, MBN and IVN

Source	Yield				MBN				IVN			
	Sum of squares	Mean square	F value	Prob> F	Sum of squares	Mean square	F value	Prob> F	Sum of squares	Mean square	F value	Prob> F
Model	1.121 x 10 ⁻⁸	1.246 x 10 ⁻⁷	25.64	< 0.0001*	1.181 x 10 ⁻³	1.181 x 10 ⁻³	34.47	< 0.0001*	1035.29	172.55	3.36	0.032*
A	9.564 x 10 ⁻⁷	9.564 x 10 ⁻⁷	196.8	< 0.0001*	3.013 x 10 ⁻⁴	3.013 x 10 ⁻⁴	79.12	< 0.0001*	47.25	47.25	0.92	0.3580
B	6.696 x 10 ⁻⁶	6.696 x 10 ⁻⁶	13.78	0.0059*	1.262 x 10 ⁻⁴	1.262 x 10 ⁻⁴	33.13	0.0004*	269.56	269.56	5.25	0.0427*
C	4.555 x 10 ⁻⁵	4.555 x 10 ⁻⁵	0.94	0.3613	2.648 x 10 ⁻⁵	2.648 x 10 ⁻⁵	6.95	0.0298*	15.47	15.47	0.30	0.5940
A ²	8.910 x 10 ⁻⁶	8.910 x 10 ⁻⁶	18.34	0.0027*	4.418 x 10 ⁻⁵	4.418 x 10 ⁻⁵	11.60	0.0093*	±	±	±	±
B ²	2.005 x 10 ⁻⁶	2.005 x 10 ⁻⁶	4.13	0.0767	1.518 x 10 ⁻⁵	1.518 x 10 ⁻⁵	0.40	0.5454	±	±	±	±
C ²	1.121 x 10 ⁻⁵	1.121 x 10 ⁻⁵	0.23	0.6438	2.900 x 10 ⁻⁶	2.900 x 10 ⁻⁶	0.76	0.4082	±	±	±	±
AB	5.362 x 10 ⁻⁶	5.362 x 10 ⁻⁶	11.03	0.0105*	3.383 x 10 ⁻⁴	3.383 x 10 ⁻⁴	88.83	< 0.0001*	497.11	497.11	9.68	0.0099*
AC	9.801 x 10 ⁻⁵	9.801 x 10 ⁻⁵	2.02	0.1933	2.844 x 10 ⁻⁵	2.844 x 10 ⁻⁵	7.47	0.0257*	32.71	32.71	0.64	0.4416
BC	45028.95	45028.95	0.093	0.7686	2.119 x 10 ⁻⁵	2.119 x 10 ⁻⁵	5.56	0.0460*	42.20	42.20	0.82	0.3840
Residual	3.887 x 10 ⁻⁶	4.859 x 10 ⁻⁵			3.046 x 10 ⁻⁵	3.808 x 10 ⁻⁶			564.71	51.34		
Lack of Fit	3.477 x 10 ⁻⁶	8.694 x 10 ⁻⁵	8.49	0.0310	3.046 x 10 ⁻⁵	7.616 x 10 ⁻⁶			564.71	80.67		
Pure Error	4.098 x 10 ⁻⁵	1.025 x 10 ⁻⁵			0.000	0.000			0.000	0.000		
Cor Total	1.160 x 10 ⁻⁸				1.212 x 10 ⁻³				1600.00			

*- significant for $p < 0.05$, ± - not applicable, A = Temperature, B = Time, C= Impregnation Ratio, IMR- impregnation ratio IVN- iodine value number MBN – methylene blue number

Only B and AB are significant model terms at $p < 0.05$. The standard deviation, mean, C.V, R², Adj R², pred R² and Adeq precision obtained for the analysis were 7.17, 76.67, 9.35, 0.6471, 0.4545, 0.0321, and 5.815, respectively. The Pred R² of 0.0321 is not as close to the Adj R² of 0.4545 as might normally be expected. This may be traced to the closeness of Adeq Precision (5.815) to a value of 4; however, the model can be used to navigate the design space, since the Adeq Precision is greater than 4.

— Model Equations Generated

The final empirical model in terms of coded factors for the responses are given by equations 16 - 18. The positive signs show favorability of the factor for increased responses while negative signs show opposition to increased responses (Alade et al., 2012b). The coefficients of A and B in eqn 17 are - 2731.75, and - 722.83, respectively, which indicate negative influence on the yield. This suggests that lower temperature and time will favour good yield (Alade et al., 2012b). High temperature and time will lead to more ashes and diminish in quality of the activated carbon (Ioannidou, and Zabaniotou, 2007). C has positive (+179.05) influence, yet all the factors have positive intercept of +475.29. Combined influence of temperature-time (+ 692.83) and time-IMR (+ 60.86) indicate positive influence, while temperature-IMR (- 283.94) combination influenced yield, negatively. The coefficients (+ 4.848 x 10⁻³ + 3.138 x 10⁻³ + 1.365 x 10⁻³) in equation (18), for MBN, indicate that temperature, time and IMR have positive influence individually, on methylene blue adsorption by the AMOP. Combined influence of temperature-time (+5.503 x 10⁻³), temperature-IMR (+1.529 x 10⁻³) and time-IMR (+1.320 x 10⁻³) along with a positive intercept of (+0.011) indicate positive influence on MBN. Temperature and impregnation ratio (+ 1.88 and + 1.04) along with a positive intercept of + 77.11, have positive

influence on the IVN (eqn 19) and the lower positive value of +1.04C shows that impregnation ratio has a lesser effect on the IVN than temperature, though it is a favourable influence while the combined influence of temperature-time, temperature-impregnation and time-impregnation (−6.66, −1.62 and − 1.84) have negative effects on the IVN.

$$(\text{Yield})^2 = +475.29 - 2731.75A - 722.83B + 179.05C + 2057.33 A^2 + 975.87 B^2 - 256.39C^2 + 692.83 AB - 283.94 AC + 60.86 BC \quad (17)$$

$$(\text{MBN})^{-1} = +0.011 + 4.848 \times 10^{-3}A + 3.138 \times 10^{-3}B + 1.365 \times 10^{-3}C + 4.581 \times 10^{-3} A^2 + 8.492 \times 10^{-4} B^2 + 1.304 \times 10^{-3}C^2 + 5.503 \times 10^{-3}AB + 1.529 \times 10^{-3}AC + 1.320 \times 10^{-3}BC \quad (18)$$

$$\text{IVN} = + 77.11 + 1.88A - 4.50B + 1.04C - 6.66AB - 1.62AC - 1.84BC \quad (19)$$

— Diagnostic Case Studies

The stacking and distribution frequencies of the results obtained for selected responses (Yield, MBN and IVN) are represented in the diagnostic plots. More stacks and distributions points exist between 40 and 70% (Figure 1a), 20 and 70% as well as, between 15 and 70%, probabilities for the normal probability graph of yield MBN and IVN, respectively. The diagnostic case studies for the percentage yield, MBN, and IVN show the residuals obtained from the difference between the actual (experiment) value and the predicted (software generated) value. Negative residual value means that the predicted value is greater than the actual value while a positive residual value suggests that the actual value is greater than the predicted value. Zero residual was obtained in cases where the predicted and actual values are equivalent (Alade et al., 2012b). The predicted versus actual plots for yield, MBN and IVN show that the closer the points to the normal line the higher the R² and vice versa. The MBN plot shows the highest R² value of 0.9848 indicating that the experimental and predicted values have a good agreement (Salman, 2014).

— Model Graphs for Yield, MBN and IVN

The relationship existing between selected factors and responses, illustrated in Figures 1a–c (3-D surface plot), were selected because of the statistical significance of time and temperature for the three selected responses (Table 3). A corresponding increase in time and temperature results in a decrease in the percentage yield of the AMOP (Figure 1). This may be ascribed to large amounts of volatile matter that are released during pyrolysis and to a lesser extent the dehydration of the precursors (Lori et al., 2008). This trend is consistent with yield model graph achieved by Salman (2014) and Lori et al., (2008). In this study with an increase in temperature from (200 - 450°C) the yield drastically decreased from 88.88 - 22.11%.

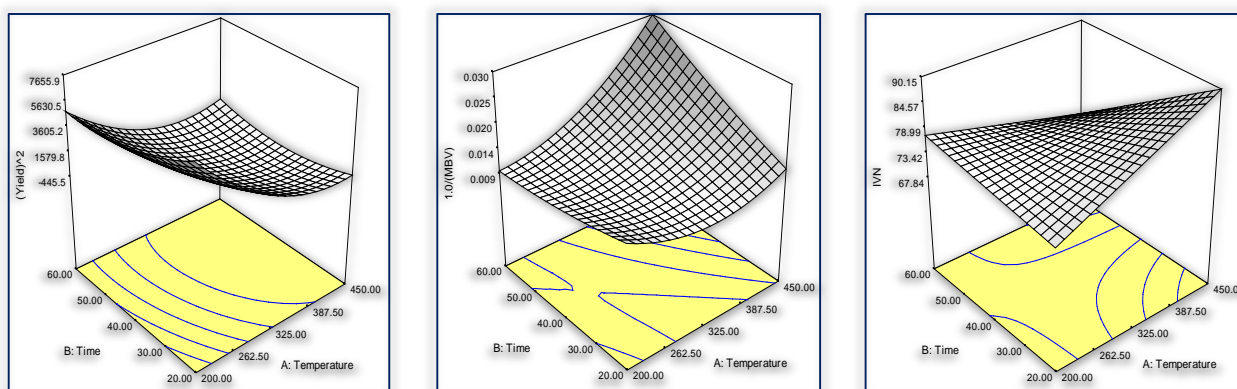


Figure 1: 3D-plot relating (a) yield, (b) MBN and (c) IVN to temperature and time

MBN value shows an increasing relationship with increase in time and temperature (Figure 1b). Characteristically, adsorption capacity of carbon to adsorb impurities tends to improve, as the temperature and the soak time increased (Ahmad et al., 2015). Foo and Hameed (2011) reported increase in MB adsorption with activation time due to better activation attained by opening inaccessible pores and formation of new pores. The highest MB removal (86.68%) in this study is in the same range as that of Okeola et al., (2012) (86.2%). Ekpete and Horsfall (2011) attribute greater adsorption capacity to high iodine value numbers. IVN plots (Figure 1c) showed that an increase in time and temperature resulted to increased IVN. In this study as temperature increased from (200 – 450 °C) the IVN increased from (78 - 96 mg/g). This implies that the pore size distributions of the AMOP changed significantly with the increasing activation temperature

resulting in more amounts of pores openings (Ma et al., 2014) and this thereby increases the adsorption capacity.

— FTIR surface characteristics of raw and activated *Moringa oleifera* pod

The FTIR analysis spectra of the raw and activated *Moringa oleifera* pod are shown in Figures 2(a-b), respectively. The IR peak observed in the raw *Moringa oleifera* pod ranged from 430.13 cm^{-1} to 3863.42 cm^{-1} , and the percentage transmittance (%T) ranged between 5 and 19, while the IR peaks observed in the AMOP ranged from 428.20 cm^{-1} to 3751.55 cm^{-1} and the percentage transmittance (%T) ranged between 5 and 22. Major changes in the IR spectra between the two samples, because of the activation were noted. Bond types such as =C-H bending and C-Br stretch bands shifted downward after activation, bond types such as C-H stretch, O-H stretch, C-C stretch and C-O stretch shifted upward after activation, while the bond types such as C-N stretch, C-Cl stretch, C-H bend, N-O asymmetric stretch and N-H bend disappeared after carbonization. The FTIR spectra of AMOP show broad peak at 3437.15 cm^{-1} and this is attributable to O-H stretch and N-H asymmetric vibrations, which could be due to inter and intra-molecular hydrogen bonding (Wuana et al., 2015).

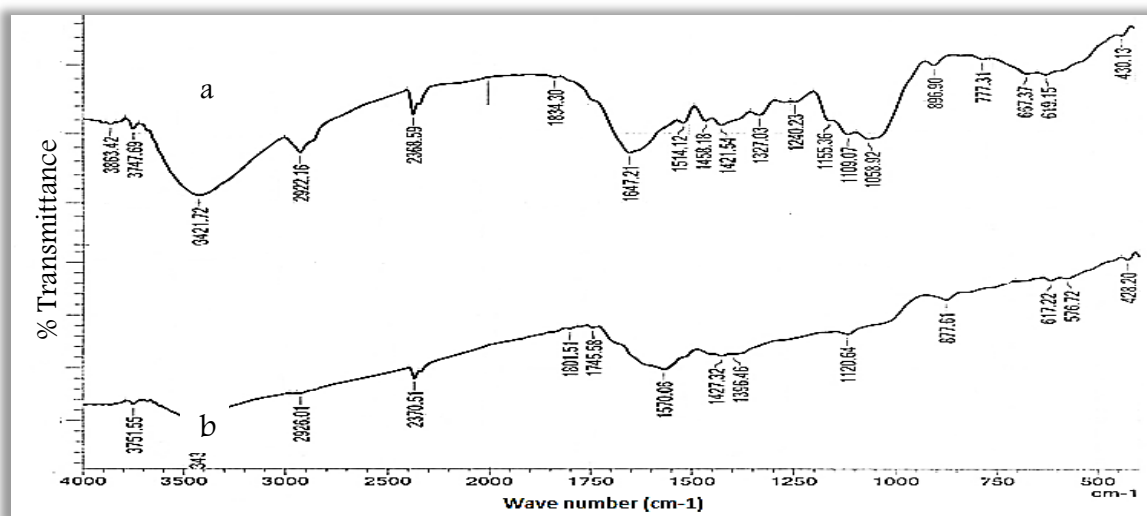


Figure 2: FTIR Spectra of (a) raw and (b) activated *Moringa oleifera* Pod

— Physicochemical Properties of Activated *Moringa oleifera* pod

The physicochemical properties for the AMOP based on the ash content, percentage moisture content, bulk density and crude fibre content in comparison with *Moringa oleifera* leave activated carbon (MLA) are related. Ash content is an indicator of the quality of an activated carbon; most commercial activated carbons have their ash contents higher than 10% (Bernardo et al., 1997). The ash content (6.44%) of AMOP compared well with the ash content of activated carbon made from coconut (5.65 %), and babassu (6.49 %) (Jaguaribe et al., 2005). High carbon and low ash content demonstrated by the AMOP, points to its potential application for the production of activated carbon (Guan et al., 2013). Moisture content (85.65 %) of the raw precursor decreased significantly to 23.05 % for AMOP. The moisture content of AMOP is higher than that of MLA (4.12 %) (Bello et al., 2015) and this may be attributed to higher tendencies of the pod back to hold more moisture than the leaf (MLA) due to differences in cellulose thickness. AMOP's bulk density (0.209 g/cm^3) is close to bulk density of 0.33 g/cm^3 obtained for H_3PO_4 -treated banana empty fruit bunch (BEFP) (Sugumaran et al., 2012). A less dense activated carbon will be able to suspend and mix in liquid medium, unlike highly dense adsorbent that may settle at the bottom, thus require high agitation and consequently, high energy.

— Process Optimisation

The maximum values obtained experimentally were optimized by the software to generate values for the responses at the highest possible desirability. The goals for temperature, time and IMR were 450, 20 and 1:1, respectively, set as 'target', while the yield, MBN, and IVN were set as 'minimise', 'maximize' and 'maximize', respectively. The optimised value for yield, MBN, and IVN were 26.8 %, 79.299 mg/g and 88.89 mg/g respectively at desirability of 0.939. The percentage error 17.5%, 17.40% and 11.65% obtained for yield, MBN, and IVN respectively, are relatively low (< 20 %) (Salman, 2014).

— **Effect of Contact Time**

Equilibrium capacity (q_e) of MB removal from the aqueous solution onto AMOP increased as the time increased. The adsorption of MB was relatively rapid within the first 40 mins and a slow uptake, which tends towards equilibrium, was displayed thereafter. Maximum adsorption capacity demonstrated by AMOP for MB adsorption is 98.46 mg/g and this compared with some commercial activated carbon as well as activated carbon derived from agricultural wastes (Srivastava et al., 2006; Fierro et al., 2008; Ozhan et al., 2014 and Kumar and Jena, 2016). The adsorption trend was fit using Microsoft software Excel statistical tools and the most suitable model equation, with highest R^2 , that can facilitate the prediction of the adsorption is given in equation 20. R^2 -value of 1.000 shows the good fitness of the equation.

$$q_e = 3 \times 10^{-8}t^5 - 1 \times 10^{-5}t^4 + 0.0022t^3 - 0.1627t^2 + 5.9645t \quad (20)$$

— **Kinetic Study**

PFO kinetic model

The parameters of PFO kinetic model obtained from the plots (Figure 3a-b) for the two linear types are shown in Table 4. The linear regression correlation (R^2) values (0.8656) obtained for the two linear types of PFO are relatively low (<0.9), as widely observed in previous studies. The experimental (q_{exp}) value (98.46 mg/g) is significantly different from the calculated (q_{cal}) value of 40.419 and 40.420 mg/g for the Type 1 and Type 2, respectively with 58.9% deviations. These observations indicate that the two types of PFO model are not suitable to predict the adsorption kinetics of MB onto AMOP. This study further suggests that either types of the PFO may be used to investigate adsorption dynamic of adsorbate in aqueous medium.

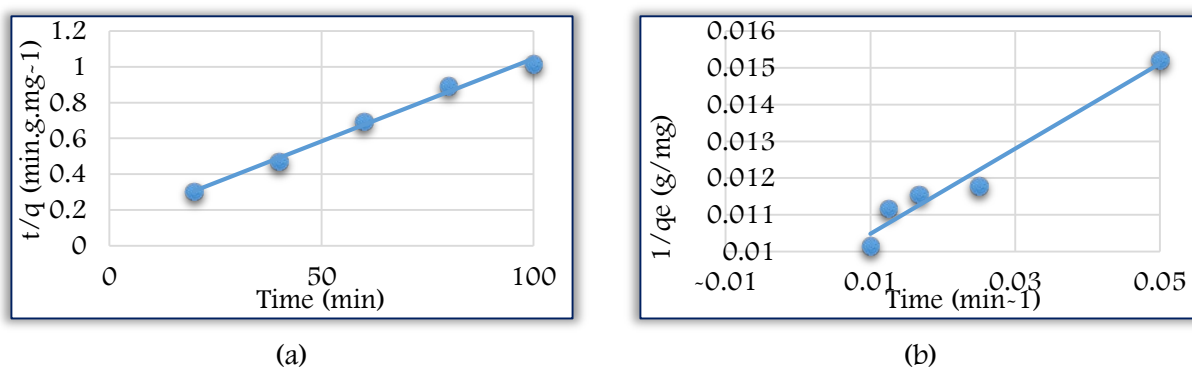


Figure 3: Plot of (a) Type1, and (b) Type2 Pseudo-First order for Methylene blue adsorption on activated Moringa oleifera Pod

PSO kinetic model

The model parameters obtained from the plots (Figure 4a-b), error analysis as well as percentage difference between the calculated (q_{cal}) and experimental (q_{exp}) are shown in Table 4. q_{cal} (106.76 mg/g) for Type 3 is the closest value to the experiment (q_{exp}) (98.46 mg/g) with 7.77% deviation, while Type 1 (108.69 mg/g) showed the widest (9.41%) deviations. Type 3 of PSO is characterized by highest rate constant (K_2) of 7.73×10^{-4} g/mg.min, while Type 4 showed the least K_2 (6.93×10^{-4}). High rate indicate faster adsorption of the adsorbate onto the surfaces of the adsorbent. These trends were further observed in the initial adsorption rate, 'h' (mg/g/min), where the highest (8.803 mg/g.min) and lowest (8.197 mg/g.min) sorption rate were demonstrated in Type 3 and Type 1, respectively. Change in the model parameter observed for the five linear expression indicate that the transformation influences the original error distribution (Baccar et al., 2015).

Type 1 has the highest R^2 of 0.9923 while Type 3 and Type 4 have the least R^2 value of 0.9139. Type 2 and Type 5 have the same R^2 value of 0.9626. Similar trend was reported by Nouri et al, (2007). The R^2 value for the five types of PSO are greater than 0.91, and thus rank all the types of PSO better than the two types of PFO linear model expressions. The choice of Type 1 as suitable model to represent the uptake of MB onto AMOP can be based on its highest R^2 value as demonstrated in most studies (Ho et al., 2002; Ho and Ofomaja, 2006). Yet the closeness of Type 3's q_{cal} to q_{exp} as well as its highest rate constant (K_2) and sorption rate (h) suggest Type 3 of linear PSO to be most suitable, scientifically, in predicting the sorption of MB onto AMOP. This study further suggests that investigation of suitability of PSO with Type 1 and Type 3 should always be observed, because high R^2 has not really taken care of the effects of the error that accompanied the transformation of non-linear PSO to its linear types (Nouri et al., 2007). Type 1 has been

predominantly and widely used linear form of to represent adsorption kinetics PSO (El-Khaiary 2010), but its error analysis is to be considered as important factor in selecting the most suitable type. Type 3 may be ranked as the most suitable PSO linear model for the adsorption of MB on AMOP. More importantly the suitability of PSO with respect to PFO, suggests that the adsorption of MB onto AMOP is controlled by chemisorption process (Hirunpraditkoon et al., 2015).

Table 4: Parameter of Pseudo-First-Order (PFO) and Pseudo-Second-Order (PSO) models

Models	Type	qe (mg·g ⁻¹)	K ₁ (min ⁻¹)	R ²	%diff		
PFO	Type 1	40.419	0.0404	0.8656	58.9		
	Type 2	40.420	0.0404	0.8656	58.9		
		qe (mg/g)	h(mg/g/mm)	R ²	%diff	Δq _c (%)	kg (g/mg/mm)
PSO	Type 1	108.695	8.197	0.9923	9.41	19.79	6.937
	Type 2	107.527	8.651	0.9626	8.43	19.07	7.482
	Type 3	106.760	8.809	0.9139	7.77	19.21	7.729
	Type 4	108.820	8.205	0.9139	9.52	19.87	6.929
	Type 5	108.410	8.326	0.9626	9.18	19.61	7.084

Elovich Kinetic Model

The available adsorption site on the AMOP for MB adsorption is given as 18.202 while the initial adsorption (α) rate is 37.40 mg/mm⁻¹. The linear plot obtained has good R² (9.9319) (Figure 4) which is better than the R² obtained for the two types of PFO as well as Type 3 and Type 4 of PSO.

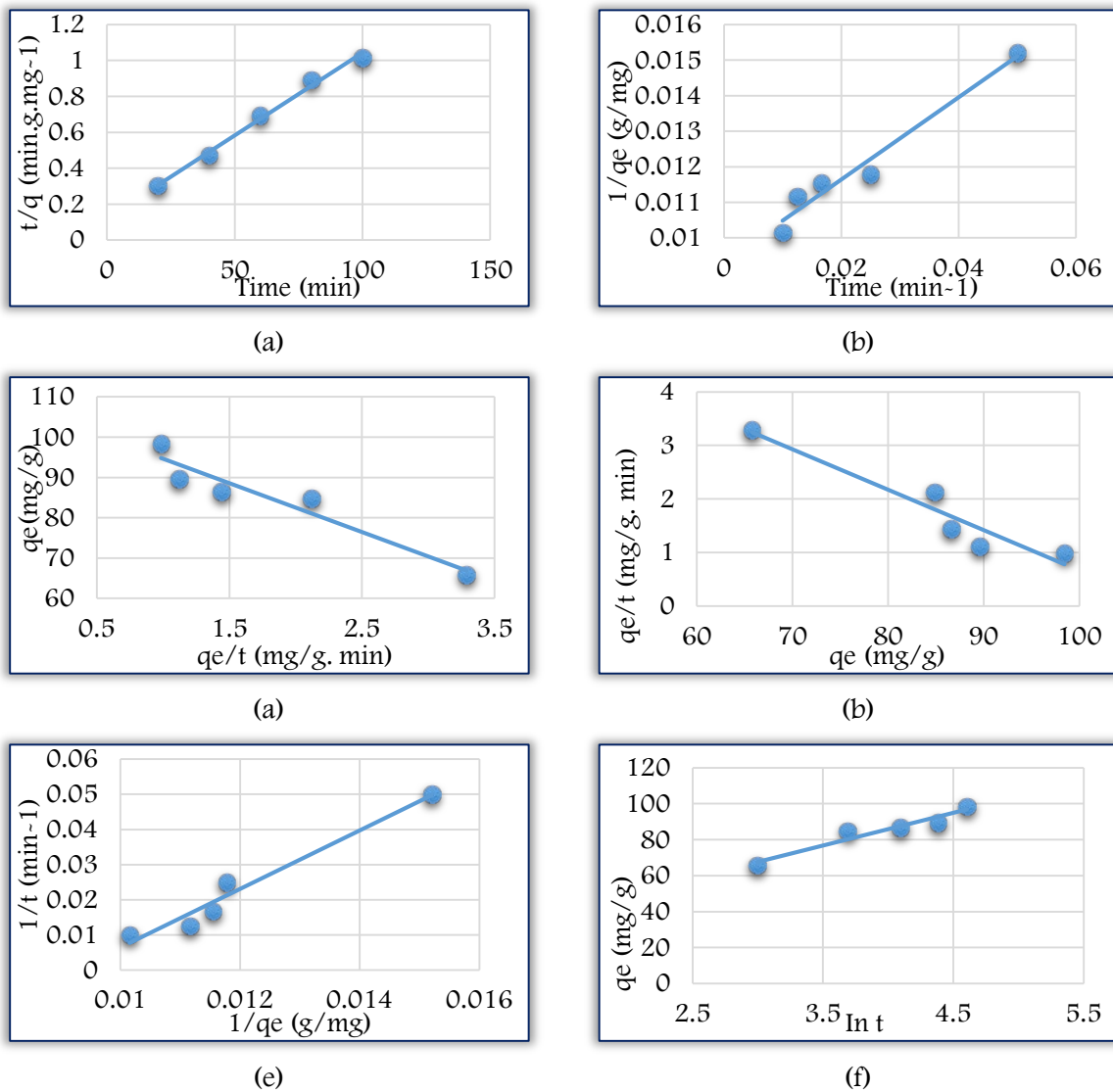


Figure 4: Plot of (a) Type1, (b) Type2, (c) Type3, (d) Type4 and (e) Type5 Pseudo-second order and (f) Elovich for Methylene blue adsorption on activated Moringa oleifera Pod

It can be deduced that Elovich model equation compares relatively with Types 3 and Type 4 of PSO, based on R² values. The error analysis, Δq_e (%), obtained for Type 1, Type 2, Type 3, Type 4, and Type 5 are 19.79, 19.09, 19.21, 19.87 and 19.61, respectively (Table 5). The order of good-fit

between the experimental and calculated data is Type 2 > Type 3 > Type 5 > Type 1 > Type 4. This trend indicates that there was less distortion of error variance while transforming PSO model equation to Type 3 linear model equation than Type 1.

— **Results of Validation**

Similar trend was reported by Subash and Prasad (2015) who used error analysis such as sum of square errors (SSE), composite fractional error function (HYBRD), derivative of Marquardt’s percent standard deviation (MPSD), average relative error (ARE), and sum of absolute errors (EABS) to rank type 1-4 linear model equations. The choice of Type 3 over Type 1 as suitable linear form of PSO to describe the kinetics of MB adsorption on AMOP is further justified.

— **Adsorption Diffusion Mechanism Models**

Weber-Morris Diffusion Model

The Weber-Morris model plot for the adsorption of MB onto AMOP displayed multi-linearity (Figure 5a). The first steep portion can be attributed to the diffusion of MB through the solution to the external surface of the AMOP (Ofomaja 2010; Doke and Khan 2012). The k_{wm} , C_{wm} and R^2 of the slope is given as $5.3769 \text{ (mgg}^{-1}\text{mm}^{-0.5}\text{)}$, 47.043 mg/g and 0.8762 , respectively (Table 5). The second gradient stage indicates slow intraparticles pore diffusion (Doke and Khan 2012) with k_{wm} , C_{wm} and R^2 of $1.6661 \text{ (mgg}^{-1}\text{mm}^{-0.5}\text{)}$, 73.448 and 0.9887 , respectively. The trend indicated that the intraparticle diffusion is the rate-limiting factor.

Table 5: Parameter for Adsorption Diffusion Mechanism Models

Model	Parameters	Value
Webber-Morris	$K_{wm1} \text{ (mgg}^{-1}\text{mm}^{-0.5}\text{)}$	5.3769
	$C_{wm1} \text{ (mg/g)}$	47.043
	R^2	0.8769
	$K_{wm2} \text{ (mgg}^{-1}\text{mm}^{-0.5}\text{)}$	1.6661
	$C_{wm2} \text{ (mg/g)}$	73.448
	R^2	0.9887
Dumwald-Wagner	$K_{WD} \text{ (mgg}^{-1}\text{min}^{-1}\text{)}$	0.02464
	R^2	0.9073
McKay	$K_M \text{ (mgg}^{-1}\text{min}^{-1}\text{)}$	0.035
	R^2	0.8290
Bangham’s	$\alpha_B \text{ (L}^2\text{/g)}$	0.228
	K_B	3.438×10^{-4}
	R^2	0.9242

Dumwald-Wagner Diffusion Model

The outlook of the plot (Figure 5b), which intersected the origin and this, suggests that film diffusion process may be the rate-controlling step in adsorption of MB onto AMOP. The diffusion rate constant obtained in this study is $0.02464 \text{ mgg}^{-1}\text{min}^{-1}$ and the R^2 -value of $0.9073 (> 0.90)$ (Table 5) suggested the suitability of the model.

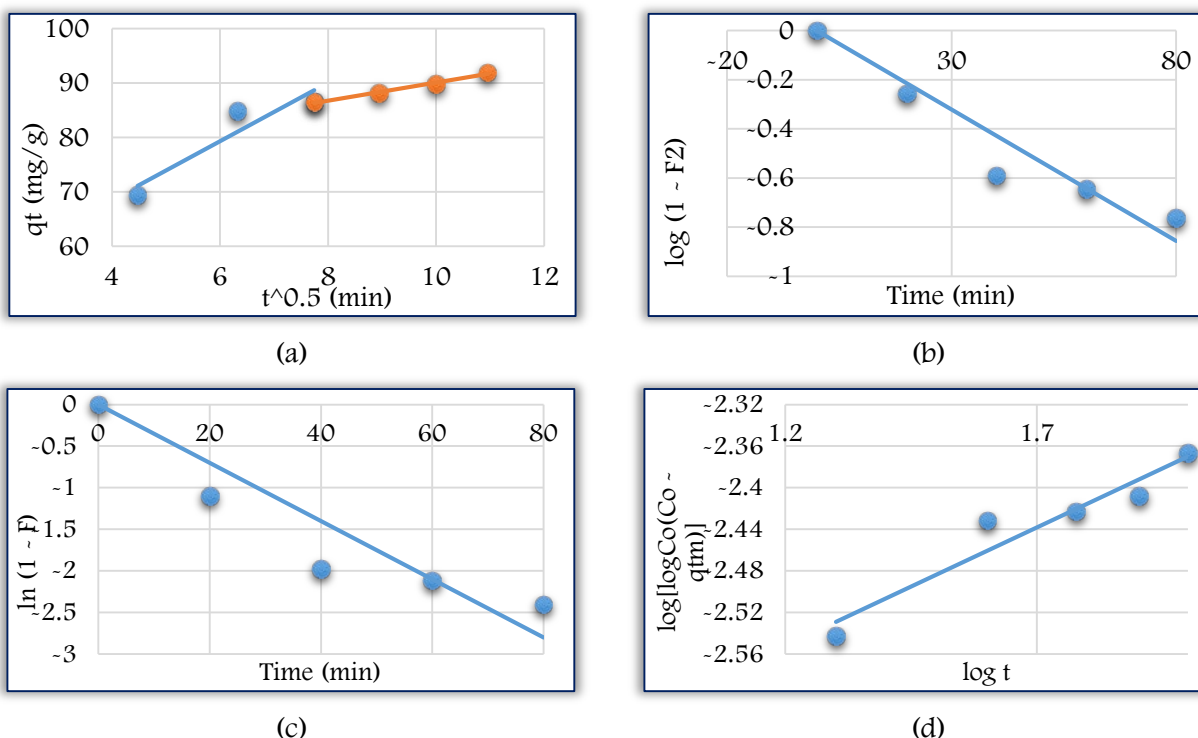


Figure 5: Plot of (a) Webber-Morris, (b) Dumwald-Wagner, (c) McKay and (d) Bangham’s Model for methylene blue adsorption on activated Moringa oleifera Pod

McKay Diffusion Model

K_M obtained for this study (Figure 5) is $0.035 \text{ mgg}^{-1}\text{min}^{-1}$ (Table 5), which is slightly higher than K_{WD} . It may be suggested that McKay model, the rate-controlling step for the adsorption of MB onto AMOP was film diffusion, since the plot did not display perfect linearity (Podder and Majumder, 2017). R^2 -value (0.829) of the McKay model is relatively low (< 0.90).

Bangham's Diffusion Model

The Bangham's model parameters, α_B and K_B , (Figure 5d), obtained for the adsorption of MB onto AMOP are $0.228 \text{ L}^2/\text{g}$ and 3.438×10^{-4} , respectively (Table 5). Suitability of the model can be based on its α_B , which is less one (< 1) (Inyinbor et al., 2016). The R^2 -value (0.9242) of the model is relatively high (> 0.90). The evaluation of the selected models for diffusion mechanism has suggested that the obvious the rate-controlling step for the adsorption MB onto AMOP is film diffusion.

5. CONCLUSION

D-Optimal Design was successfully employed to produce effective activated carbon from moringa oleifera pod (AMOP). Optimum conditions for activation/carbonization process based on yield (22.1%), IVN (96 mg/g) and MBN (78.53 mg/g) values are $450 \text{ }^\circ\text{C}$, 20 mins and impregnation ratio of 1:1. The experimental values obtained for the MB dye removal, with deviation errors less 20 %, agreed satisfactorily with the values predicted by the models. The differences in the functional groups characterised on the surfaces of the raw and AMOP indicated the influence of the selected factors and processes on the properties of the activated carbon produced. Rate of MB adsorption fitted well to Type 3 linear form of pseud-second-order kinetic model and the selected diffusion mechanism models indicate film diffusion as the rate-controlling step for the adsorption MB onto AMOP. The closeness of these properties to other effective activated carbon derived from agricultural wastes suggest moringa Oleifera pod as potential precursor for production of effective adsorbent for the removal of MB pollutants from wastewater.

Acknowledgement

The research is supported by fund of the No3, Batch 7 of TETFund 2014 Research Project [RP] Intervention for Ladoko Akintola University of Technology (LAUTECH), Ogbomosho, Nigeria.

References

- [1] Abdel-Ghani N.T., El-Chaghaby G.A.F., and Hefny M. Removal of lead from aqueous solution using low cost abundantly available adsorbents, *International Journal of Environmental Science Technology*, 4 (1):67–73 (2007).
- [2] Ahmad, M.A., Ahmad, N., and Bello, O.S. Adsorption Kinetic Studies for the Removal of Synthetic Dye Using Durian Seed Activated Carbon. *Journal of Dispersion Science and Technology*, 36:670–684, 2015
- [3] Alade, A.O., Amuda, O.S., Afolabi T J, and Okoya, A. Adsorption of Naphthalene onto activated carbon derived from milk bush kernel shell and flamboyant pod. *Journal of Environment Chemistry and Ecotoxicology*, 4(7): 124-132(2012a)
- [4] Alade, A.O., Amuda, O.S., Ogunleye, O., and Okoya, A. Evaluation of Interaction of Carbonization Temperatures and Concentrations on the Adsorption Capacities and Removal Efficiencies of Activated Carbons Using Response Surface Methodology (RSM). *Journal of Bioremediation and Biodegradation*, 3:134. doi:10.4172/2155-6199.1000134. (2012b)
- [5] Amuda, O.S., Olayiwola, A.O., Alade, A.O., Farombi, A.G. and Adebisi, S.A. Adsorption of Methylene Blue from Aqueous Solution Using Steam-Activated Carbon Produced from Lantana camara Stem. *Journal of Environmental Protection*, 5:1352-1363. (2014).
- [6] Anirudhan, T.S., and Sreekumari, S. Adsorptive removal of heavy metal ions from industrial effluents using activated carbon derived from waste coconut buttons, *Journal of Environmental Sciences*, 23(12):1989–1998. (2011).
- [7] Arora, D.S., Onsare, J.G., and Kaur H. Bioprospecting of Moringa (Moringaceae): Microbiological Perspective. *Journal of Pharmacognosy and Phytochemistry*, 1(6):193 – 215 (2013).
- [8] Baccar, R., Blázquez, P., Bouzid, J., Feki, M., Attiya, H., and Sarra, M., Modeling of adsorption isotherms and kinetics of a tannery dye onto an activated carbon prepared from an agricultural by-product. *Fuel Processing Technology* 106 (13) 408–415 (2015).
- [9] Baker, F.S., Miller, C.E., Repic, A.J., and Tolles, E.D. Activated carbon. *Kirk-Othmer Encyclopedia of Chemical Technology*. 4:1015-1037. (1992).
- [10] Bello, O.S., Kayode, B., Adegoke, A., and Omowumi, O. Preparation and characterization of a novel adsorbent from Moringa oleifera leaf. *Applied Water Science*, 1:1-11. (2015).
- [11] Bernardo, E.C., Egashira, R., and Kawasaki, J. Decolourization of Molasses' Wastewater Using Activated Carbon Prepared from Cane Bagasse. *Carbon* 35(9):1217-1221. (1997).

- [12] Blanchard, G., Maunaye, M. and Martin, G. Removal of heavy metals from waters by means of natural zeolites. *Water Res.* 18::1501–1507. (1984).
- [13] Doke, K.M., and Khan, E.M. Equilibrium, kinetic and diffusion mechanism of Cr(VI) adsorption onto activated carbon derived from wood apple shell. *Arabian Journal of Chemistry*. <http://dx.doi.org/10.1016/j.arabjc.2012.07.031>.DOI.S1878535212001906. (2012).
- [14] Ekpete, O.A., and Horsfall, M. Preparation and Characterization of Activated Carbon derived from Fluted Pumpkin Stem Waste (*Telfairia occidentalis* Hook F). *Research Journal of Chemical Science*. 1(3):10-17. (2011).
- [15] El-Hendawy, A. Influence of HNO₃ oxidation on the structured and adsorptive properties of corncob activated carbon. *Carbon*, (2003).41:713-722 (2003).
- [16] El-Khaiary, M.I., Malash, G.F. and Ho, Y-S. On the use of linearized pseudo-second-order kinetic equations for modeling adsorption systems *Desalination* 257: 93–101 (2010).
- [17] Foo, K.Y., and Hameed, B.H. Preparation and characterization of activated carbon from sunflower seed oil residue via microwave assisted K₂CO₃ activation. *Bioresource Technology*, 102: 9794-9799. (2011)
- [18] Garcia, F.S., Alonso, A.M., and Tascon, J.M.D. Porous texture of activated carbons prepared by phosphoric acid activation of apple pulp. *Carbon* 39:1103-1116. (2003).
- [19] Gimba, C, and Musa, I. Preparation of activated carbon from agricultural waste: cyanide binding with activated carbon matrix from coconut shell. *Nigerian Journal of Chemical Research*. 32:167–170 (2007).
- [20] Guan, B.T.H., Abdul Latif, P., and Yap, T.Y.H. Physical Preparation of Activated Carbon from Sugarcane Bagasse and Corn Husk and Its Physical and Chemical. *International Journal of Engineering Research and Science and Technology*, 2(3): 1–14. (2013).
- [21] Hashem, M.A. Adsorption of lead ions from aqueous solution by okra wastes, *International Journal of Physical Science*. 2 (7):178–184 (2007).
- [22] Hesas, R.H., Arami-niya, A., Mohd, W., Wan, A., and Sahu, J.N. Preparation and Characterization of Activated Carbon. *BioResources*, 8(2):2950–2966 (2013).
- [23] Hirunpraditkoon, S., Srinophakun, P., Sombun, N., and Moore, E.J. Synthesis of Activated Carbon from *Jatropha* Seed Coat and Application to Adsorption of Iodine and Methylene Blue. *Chemical Engineering Communications*, 202:32–47 (2015).
- [24] Ho Y.S., Porte R.J.F., and McKay G. Equilibrium isotherm studies for the sorption of divalent metal ions onto peat: copper, nickel and lead single component systems. *Water, Air, and Soil Pollution*. 141:1–33(2 002)
- [25] Ho, Y.S. and Ofomaja, A.E. Biosorption thermodynamics of cadmium on coconut copra meal as biosorbent, *Biochem. Eng. J.* 30:117–123. (2006).
- [26] Ho, Y.S., and McKay, G. The kinetics of sorption of divalent metal ions onto sphagnum moss peat. *Water Res.* 34:735–742. (2000).
- [27] Inyinbor, A.A., Adekola, F.A., and Olatunji, G.A. Kinetics, isotherms and thermodynamic modeling of liquid phase adsorption of Rhodamine B dye onto *Raphia* okerie fruit epicarp. *Water Resources and Industry* 15:14–27 (2016).
- [28] Ioannidou, O., and Zabaniotou, O. Agricultural residues as precursors for activated carbon production – A review. *Renewable and Sustainable Energy Reviews* 11:1966 – 2002 (2007)
- [29] Jaguaribe, E.F., Medeiros, L., Barreto, M.C.S., and Araujo, L.P. The performance of activated carbons from sugarcane bagasse, babassu, and coconut shells in removing residual chlorine. *Brazilian Journal of Chemical Engineering*. 22(1): 41–47 (2005)
- [30] Kabore A, Savadogo B, Rosillon F, Traore A S, and Dianou D. Effectiveness of *Moringa oleifera* Defatted Cake versus Seed in the Treatment of Unsafe Drinking Water: Case Study of Surface and Well Waters in Burkina Faso. *Journal of Water Resource and Protection*, 5:1076-1086. (2013).
- [31] Lilliehöök H. Use of Sand Filtration on River Water Flocculated with *Moringa oleifera*, Division of Sanitary Engineering, Department of Civil and Environmental Engineering, Luleå University of Technology, ISBN: LTU-EX- -05/177- - SE. (2005)
- [32] Lori J A, Lawal A.O, Ekanem E J. Active carbons from chemically mediated pyrolysis of agricultural wastes: Application in simultaneous removal of binary mixture of benzene and Toluene from water. *International Journal of Environmental Research*, 2(4), 411–418 (2008).
- [33] Lua A C, Yang T, and Guo J. Effects of pyrolysis conditions on the properties of activated carbons prepared from pistachio-nut shells. *Journal of Analytical and Applied Pyrolysis*, 72: 279-287 (2004).
- [34] Ma X, Yang H, Yu L, Chen Y, and Li Y. Preparation, Surface and Pore Structure of High Surface Area Activated Carbon Fibers from Bamboo by Steam Activation. *Materials*, 7(6): 4431–4441(2014).
- [35] McConnachie G L, Warhurst A M, Pollard S J, and Chipofya, V. Activated carbon from *Moringa* husks and pods, 22nd WEDC Conference, Reaching the unreached: challenges for the 21st Century, New Delhi, India, p.279–282. (1996)
- [36] McKay, G., Otterburn, M.S., and Sweeny, A.G. Surface mass transfer process during colour removal from effluents using silica. *Water Res* 15:321–331. (1981)

- [37] Muyibi, S.A., Ameen, E.S.M., Noor, M.J.M., and Ahmadum, F.R. Bench Scale Studies for Pretreatment of Sanitary Landfill Leachate with *Moringa oleifera* seed Ex- tract. *International Journal of Environmental Studies*. 59 (5):513-535. (2002).
- [38] Njoku, V.O., Foo, K.Y., Asif, M., and Hameed, B.H. Preparation of activated carbons from rambutan (*Nephelium lappaceum*) peel by microwave-induced KOH activation for acid yellow 17 dye adsorption. *Chemical Engineering Journal*, 222:108–119. (2014).
- [39] Nouri, L., Ghodbane, I., Hamdaoui, O., and Chiha, M. Batch sorption dynamics and equilibrium for the removal of cadmium ions from aqueous phase using wheat bran. *J. Hazard. Mater.* 149:115–125. (2007).
- [40] Okeola, O.F., Odebunmi, E.O., and Ameen O. Comparison of sorption capacity and surface area of activated carbon prepared from *Jatropha curcas* fruit pericarp and seed coat. *Bulletin of the Chemical Society of Ethiopia*, 26(2), 171–180. (2012).
- [41] Podder, M.S. and Majumder, C.B. Kinetic, mechanistic and thermodynamic studies of removal of arsenic using *Bacillus arsenicus* MTCC 4380 immobilized on surface of granular activated carbon/MnFe₂O₄ composite. *Groundwater for Sustainable Development* 2-3:53–72. (2016).
- [42] Rafatullah, M., Sulaiman, O., Hashim, R., and Ahmad, A. Adsorption of methylene blue on low-cost adsorbents: a review. *Journal of Hazardous Materials*, 177: 70–80. (2010).
- [43] Rashidzadeh, A., Olad, A., and Salari, D. The effective removal of methylene blue dye from aqueous solutions by NaAlg-g-poly(acrylic acid-co-acryl amide)/clinoptilolite hydrogel nanocomposite. *Fibers and Polymers*, 16(2), 354– 362. (2015).
- [44] Salman, J.M. Optimization of preparation conditions for activated carbon from palm oil fronds using response surface methodology on removal of pesticides from aqueous solution. *Arabian Journal of Chemistry*, 7:101-108 (2014).
- [45] Sarpong, G., and Richardson, C.P. Coagulation efficiency of *Moringa oleifera* for removal of turbidity and reduction of total coliform as compared to aluminum sulfate. *African Journal of Agricultural Research*, 5(21):2939-2944(2010).
- [46] Sharma, P., Kumari, P., Srivastava, M., and Srivastava, S. Removal of cadmium from aqueous system by shelled *Moringa oleifera* Lam. seed powder. *Bioresource Technology*, 97:299–305. (2006).
- [47] Sharma, P., Kumari, P., Srivastava, M., and Srivastava, S. Ternary biosorption studies of Cd (II), Cr (III) and Ni (II) on shelled *Moringa oleifera* seeds. *Bioresource Technology*, 98:474–477. (2007).
- [48] Sivakumar, D. Adsorption study on municipal solid waste leachate using *Moringa oleifera* seed. *International Journal of Environmental Science and Technology*, 10(1):113–124 (2013).
- [49] Subash, N., and Prasad, R.K. Kinetics and mass transfer models for sorption of titanium industry effluent in activated carbon. *Desalination and Water Treatment*, DOI:10.1080/19443994.2015.1016458. (2015)
- [50] Sugumaran, P., Susan, V.P., Ravichandran, P., and Seshadri, S. Production and Characterization of Activated Carbon from Banana Empty Fruit Bunch and *Delonix regia* Fruit Pod. *Journal of Sustainable Energy and Development*, 3:125–132. (2012)
- [51] Verla, A.W., Horsfall (Jnr), M., Verla, E.N., Spiff, A.I., and Ekpete, O.A. Preparation and Characterization of activated carbon from fluted pumpkin (*telfairia occidentalis* hook. f) seed shell. *Asian Journal of Natural and Applied Science*, 1(3):39-50. (2012).
- [52] Weber, W.J., and Morris, J.C. Kinetics of adsorption on carbon from solution. *J. Sanitary Eng. Div. Am. Soc. Civil Eng.* 89:31–59. (1963)
- [53] Wuana, R.A., Ato, R.S., and Iorhen, S. Aqueous phase removal of floxacillin using adsorbents from *Moringa oleifera* pod husks. *Advances in Environmental Research*, 4(1):49–68 (2015).



ANNALS of Faculty Engineering Hunedoara – International Journal of Engineering
ISSN 1584 - 2665 (printed version); ISSN 2601 - 2332 (online); ISSN-L 1584 - 2665
copyright © University POLITEHNICA Timisoara,
Faculty of Engineering Hunedoara,
5, Revolutiei, 331 128, Hunedoara, ROMANIA
<http://annals.fih.upt.ro>